PAPER

Diffraction of vortex Gaussian beams from a two-dimensional Raman-induced grating

IOP Publishing | Astro Ltd Laser Physics

Laser Phys. **31** (2021) 065401 (9pp) https://doi.org/10.1088/1555-6611/abf567

Diffraction of vortex Gaussian beams from a two-dimensional Raman-induced grating

V G Arkhipkin[1,2,*] **and S A Myslivets**[1,2,*]

[1] Kirensky Institute of Physics, Federal Research Center KSC SB RAS, 660036 Krasnoyarsk, Russia
[2] Department of Photonics and Laser Technology, Siberian Federal University, Krasnoyarsk 660041, Russia

E-mail: avg@iph.krasn.ru and sam@iph.krasn.ru

Received 1 March 2021
Accepted for publication 3 April 2021
Published 27 April 2021

Abstract

In this paper, we study diffraction of a vortex Gaussian probe beam on a two-dimensional (2D) Raman-induced diffraction grating. Both near- and far-field diffraction of a vortex beam is considered. In the near field, quasi-Talbot images occur at specific distances from the grating, which corresponds to the classical Talbot length. Diffraction patterns in the Talbot planes are a periodic 2D array of ring-like vortex beamlets with topological charges (TCs) equal to the illuminating probe beam's charge. The lateral (off-axis) beamlets consist of several overlapping vortices with the TCs $l = 1$ and $l = -1$, and their centers (singular points) are offset relative to each other. It is shown that in the near field the TC is conserved, and the total diffraction field represents a single (global) vortex with an effective TC equal to the charge of the vortex probe beam. In the far field, diffraction patterns are also a 2D array of ring-like local vortices with a period depending on the z coordinate. Their TCs are equal to the charge of the probe field. It is shown that in a far field, the diffracted field's total TC is also equal to that of the probe field. We demonstrate that by choosing the pump field parameters, one can effectively control the intensity of diffraction orders.

Keywords: diffraction, Raman gain, Talbot effect, optical vortex beam

(Some figures may appear in colour only in the online journal)

1. Introduction

The optical vortex (also referred to as vortex beams or phase singularity beams) is an optical wave-field that carries a phase singularity where both the real and imaginary values of the optical field go to zero, and the phase is undefined [1]. Such a beam of light carries an orbital angular momentum (OAM) [2] and its transverse intensity profile looks like a ring of light with a dark core at the center. Also, there are optical vortices without circular symmetry [3, 4]. In addition to OAM, optical vortices are characterized by a topological charge (TC) [1]. At present, optical vortices are of great interest and actively studied in optics [1, 5, 6]. A number of methods have been proposed to generate phase singularity beams [2, 7, 8]. Studying the light with phase singularities is important from the viewpoint of fundamental and applied physics [9]. In the past three decades, there has been remarkable progress in understanding vortex beams' nature, and in their production and use [10]. Optical vortices have found many interesting applications in different areas. In particular, light beams with phase singularities can be used in optical communications [11], super-resolution microscopy [12], atom guiding and trapping [13], particle manipulation (optical tweezers) [14], quantum information technologies [15], etc.

Fresnel and Fraunhofer diffraction of singular beams from different apertures and periodic structures are an active

* Authors to whom any correspondence should be addressed.

research area in optical physics [16–19]. Even at simple apertures, diffraction of vortex beams exhibits unusual features, which depart from the plane waves. Diffraction of vortex beams by structured apertures is a promising method to determine the magnitude and sign of TCs [20, 21]. Also, diffraction of such beams from gratings [22–24], as well as the Talbot effect [25] are used for the same measurements. Diffraction by two-dimensional (2D) gratings makes it possible to obtain 2D arrays of optical vortices both in the far [26], and in the near field [27, 28]. It is shown that in the latter case, no self-images of the grating are observed, however at certain distances that correlate with the 'Talbot distances' for ordinary light, there are observed periodic structures with unusual amplitude and phase distributions.

Conventional diffraction gratings usually have non-tunable parameters since they have fixed configurations. Over the recent years, important progress has been made toward the realization of optical tunable gratings based on electromagnetically induced gratings in atomic media (EIG) [29], which are based on the phenomenon of electromagnetically induced transparency in the field of a standing control wave. Here a periodic structure is created by externally controlled light, and non-material gratings with optically tunable parameters are obtained [30–32]. Diffraction of light via EIGs can also be applied to create the electromagnetically induced Talbot effect [33], which would be very useful for imaging 2D ultra-cold atoms [34]. Clearly, tunable diffraction gratings have more promising applications.

Another type of EIG is a Raman-induced grating (RIG) [35, 36] with the probe field operating in a stimulated Raman emission mode to eliminate the signal attenuation. Unlike the EIG schemes, where absorption is spatially modulated, RIG is based on the Raman gain's spatial modulation by using a standing-wave pump field. RIG can work as a diffraction grating when the probe field propagates along the direction normal to the standing wave [37]. In this case, RIG will be called a Raman-induced diffraction grating (RIDG). The principal advantage of RIDG is that under certain conditions, the probe wave can diffract into many higher-order directions with amplification. The intensity of diffracted beams can be higher than that of the input beam. This paper presents a comprehensive analytical study of diffraction of a vortex Gaussian probe beam with an arbitrary value of the TC l at a 2D RIDG. The diffraction cases in both near-field (Fresnel) and far-field (Fraunhofer) diffraction are considered.

2. Diffraction of vortex Gaussian beams from 2D RIDG

RIG arises from Raman interaction of a weak probe wave with the frequency ω_2 with a standing pump wave with the frequency ω_1 in an atomic Λ-system (figure 1(a)) [35, 36]. This is due to periodic spatial modulation of the Raman amplification and the refractive index of the probe field. For a 2D grating, the pump field is formed by two orthogonal standing waves of the same frequency that are directed along the x and y axes, and the probe field propagates normal to the x–y plane in the region of the intersection of two orthogonal standing waves. The pump standing fields consist of two fields propagating at $\theta_{1,2}$ angles symmetrically to the z direction (figure 1(b)) The standing waves have the periods $d_x = \lambda_1/2\sin(\theta_1/2)$ and $d_y = \lambda_1/2\sin(\theta_2/2)$ along the axes x and y, which can be made arbitrarily larger than the wavelength of the pump fields by varying θ_1 and θ_2.

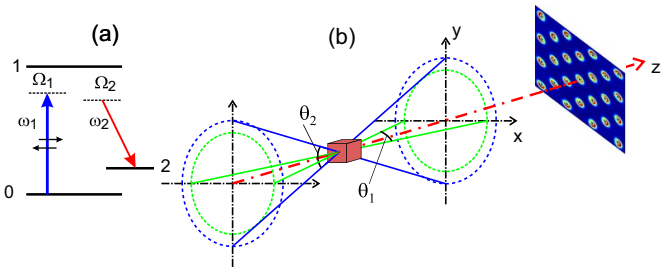

Figure 1. (a) A three-level Λ-type atomic system for a Raman induced grating. Here $\Omega_1 = \omega_1 - \omega_{10}$, $\Omega_2 = \omega_2 - \omega_{12}$, and $\omega_{10,12}$ are the frequencies of the transitions $|1\rangle - |0\rangle$ and $|1\rangle - |2\rangle$, respectively. (b) Configuration of a standing-wave pump field.

Here we will consider the probe field to be a Gaussian vortex beam. In Cartesian coordinates, the complex amplitude of a probe beam $E_2(x_0, y_0, 0)$ in the input grating plane $z_0 = 0$ can be written as

$$E_2(x_0, y_0, 0) = E_{02}\left(\frac{x_0 + isy_0}{w}\right)^{|l|} \exp\left(-\frac{x_0^2 + y_0^2}{w^2}\right), \quad (1)$$

where l is the TC, w is the vortex beam radius parameter for which the intensity maximum occurs at an effective radius of $w_{\text{eff}} = w\sqrt{|l|/2}$. The parameter $s = \pm 1$ for the positive or negative l, respectively. Further we will consider $l > 0$. Behind the grating, at $z_0 = L$, the wave will be transformed by the grating to become

$$E_2(x_0, y_0, L) = T(x_0, y_0, L)E_2(x_0, y_0, 0), \quad (2)$$

where $T(x_0, y_0, L) = \exp(-ik_2\chi(\omega_2)L)$ is the grating transmission function. Here $\chi(\omega_2)$ is the probe field susceptibility (see appendix). For a 2D grating the transmission function $T(x_0, y_0, L)$ will be periodic in the x and y directions $T(x_0, y_0, L) = T(x_0 + \Lambda_x, y_0, L) = T(x_0, y_0 + \Lambda_y, L)$ with the period $\Lambda_{x,y} = 2d_{x,y}$. The transmission function $T(x_0, y_0, L)$ of RIDG depends on the Rabi frequency of the pump field G_1 and the detuning from the Raman resonance $\Omega_{20} = \Omega_1 - \Omega_2$. Figure 2 shows two typical profiles for the transmission function module $|T|$ of a 2D grating. The parameter G_1 is chosen such that in the former case there is no spatial splitting in $|T(x_0, y_0, L)|$ (figure 2(a)), whereas in the latter case, the transmission $|T(x_0, y_0, L)|$ is split (figure 2(b)). In the latter case, the intensity distribution has a glass-like structure. It can be seen that for a 2D grating, the period in the x and y directions has doubled compared to the standing pump wave.

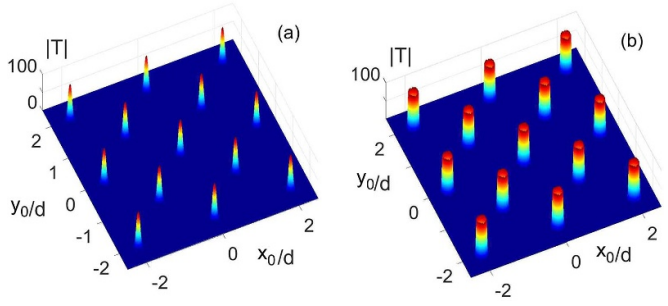

Figure 2. Typical profiles of the transmission function module $|T|$ (a) and phase ϕ (b) for a 2D RIDG. $G_1 = 0.865\gamma_{10}$, $\Omega_{20} = 30\gamma_{20}$. $d = d_x = d_y$ is the period of a standing wave.

2.1. Fresnel diffraction of the vortex beam from a 2D RIDG (near-field approximation)

The amplitude of a diffracted probe light beam $E_2(x,y,z)$ having propagated a distance of $z = z_0 - L$ from the grating output plane, can be calculated by using the Fresnel integral as follows [38].

$$E_2(x,y,z) = \frac{\exp(ik_2 z)}{i\lambda_2 z} \iint_{-\infty}^{\infty} E_2(x_0,y_0;L) \times \exp\left[i\frac{k_2}{2z}[(x-x_0)^2 + (y-y_0)^2]\right] dx_0 dy_0. \quad (3)$$

Equation (3) can be rewritten as

$$E_2(x,y,z) = E_{02}\frac{\exp[ik_2 z + i(k_2/2z)(x^2+y^2)]}{i\lambda_2 z w^l} \times \iint_{-\infty}^{\infty} T(x_0,y_0;L)(x_0+iy_0)^l \times \exp\left[-\alpha(x_0^2+y_0^2) - i\frac{k_2}{z}(xx_0+yy_0)\right] dx_0 dy_0, \quad (4)$$

where $\alpha = (1 - ik_2 w^2/2z)/w^2$. Since the grating transmission function is periodic in the x and y directions with the periods Λ_x and Λ_y, $T(x_0,y_0,L)$ can be expanded into a 2D Fourier series

$$T(x_0,y_0;L) = \sum_{n,m} t_{nm} \exp[i2\pi(nG_x x_0 + mG_y y_0)], \quad (5)$$

where $G_x = 1/\Lambda_x$ and $G_y = 1/\Lambda_y$, t_{nm} are the Fourier coefficients which can be calculated as follows:

$$t_{nm} = \frac{1}{\Lambda_x \Lambda_y} \int_{-\Lambda_y/2}^{\Lambda_y/2} \int_{-\Lambda_x/2}^{\Lambda_x/2} T(x_0,y_0;L) \times \exp\left[-i2\pi(nG_x x_0 + mG_y y_0)\right] dx_0 dy_0. \quad (6)$$

The analysis shows that the Fourier coefficients t_{nm} are nonzero only if n and m have the same parity. In addition, the relation $t_{n,m} = t_{m,n} = t_{-n,-m} = -t_{-n,m} = -t_{n,-m}$ is fulfilled. These properties will be used later in the analysis of the results.

Using a binomial expansion, the function $(x_0 + iy_0)^l$ can be rewritten as

$$(x_0 + iy_0)^l = \sum_{q=0}^{l} \binom{l}{q} x_0^q (iy_0)^{l-q}, \quad (7)$$

where $\binom{l}{q} = \frac{l!}{q!(l-q)!}$ are the binomial coefficients. Now, using equations (5) and (7) in equation (4) we get

$$E_2(x,y,z) = E_{02}\frac{\exp[ik_2 z + i(k_2/2z)(x^2+y^2)]}{i\lambda_2 z w^l} \times \sum_{n,m} t_{nm} \sum_{q=0}^{l} \binom{l}{q} (i)^{l-q} \iint_{-\infty}^{\infty} dx_0 dy_0 \times x_0^q \exp\left[-\alpha x_0^2 + i\left(2\pi n G_x - \frac{k_2}{z}x\right)x_0\right] \times y_0^{l-q} \exp\left[-\alpha y_0^2 + i\left(2\pi n G_y - \frac{k_2}{z}y\right)y_0\right]. \quad (8)$$

The integrals of both x_0 and y_0 can be calculated using the following reference integral [39]

$$\int_{-\infty}^{\infty} u^m \exp(-au^2 - bu)du = \pi^{1/2}\left(\frac{i}{2}\right)^m a^{-(m+1)/2} \times \exp\left(\frac{b^2}{4a}\right) H_m\left(\frac{ib}{2a^{1/2}}\right), \quad (9)$$

where H_m is the Hermite polynomial, and the result is

$$E_2(x,y,z) = -i\left(-\frac{1}{2}\right)^l \frac{\pi w^{l+2}}{\lambda_2 z(1-ia)^{l+1}} \times E_{02}\exp[ik_2 z + i(k_2/2z)(x^2+y^2)] \times \sum_{n,m} t_{nm}(b_{xn} + ib_{ym})^l \exp\left[-\frac{(b_{xn}^2 + b_{ym}^2)w^2}{4(1-ia)}\right]. \quad (10)$$

Here $b_{xn} = 2\pi n G_x - k_2 x/z$ and $b_{ym} = 2\pi m G_y - k_2 y/z$, $a = k_2 w^2/2z = \pi w^2/\lambda_2 z$. Therefore, the total diffracted field is represented as the sum of diffraction orders (zeroth, positive, and negative). Each spatial harmonic has a singular point, which is determined by the condition: $b_{xn} = 2\pi n G_x - k_2 x/z = 0$ and $b_{ym} = 2\pi m G_y - k_2 y/z = 0$. In particular, for the first Talbot plane, the $x-y$ coordinates of these points are defined as $x = 2m\Lambda_x$ and $y = 2n\Lambda_y$. But singular points in the diffracted field are determined by interference of all harmonics and their position may not match with the singularities of individual spatial harmonics. The intensity and phase profiles of the diffracted field can be calculated by equation (10). The TC l can be found from the formula [1]

$$l = \frac{1}{2\pi}\oint_C \nabla\psi(x,y)dxdy, \quad (11)$$

where $\psi(x,y)$ is the phase of the diffracted field $E_2(x,y,z)$. The integration contour C covers the region wherein singular

points are contained. Note that if multiple vortices are enclosed in the contour C, their TCs are additive.

2.2. Fraunhofer diffraction of a vortex beam from a 2D RIDG (far-field approximation)

Now we consider the far-field approximation, that takes place when z satisfies the condition

$$\frac{k_2}{2z}(x_0^2+y_0^2)_{\max}=\frac{\pi(x_0^2+y_0^2)_{\max}}{\lambda_2 z}\ll 1. \tag{12}$$

In this case the term $\alpha(x_0^2+y_0^2)$ can be eliminated in equation (4), and the latter reduces to [38]

$$\begin{aligned}E_2(x,y,z)=E_{02}\frac{\exp[ik_2z+i(k_2/2z)(x^2+y^2)]}{i\lambda_2 z w^l}\\ \times\iint_{-\infty}^{\infty}T(x_0,y_0,L)(x_0+iy_0)^l\exp\left(-\frac{x_0^2+y_0^2}{w^2}\right)\\ \times\exp\left[-i\frac{k_2}{z}(xx_0+yy_0)\right]dx_0dy_0.\end{aligned} \tag{13}$$

Like in the near-field approximation, here again, we can calculate the integrals in equation (13) and get

$$\begin{aligned}E_2(x,y,z)=-i\left(-\frac{1}{2}\right)^l\frac{\pi w^{l+2}}{\lambda_2 z}\\ \times E_{02}\exp[ik_2z+i(k_2/2z)(x^2+y^2)]\\ \times\sum_{n,m}t_{nm}(b_{xn}+ib_{ym})^l\exp\left[-\frac{(b_{xn}^2+b_{ym}^2)w^2}{4}\right].\end{aligned} \tag{14}$$

The diffracted complex amplitude can be determined using this equation. Formula (14) formally follows from (10) under the condition $a=k_2w^2/z\ll 1$, which can be considered as a criterion of the far-field approximation.

3. Results and discussion

We use sodium atoms as a medium where the grating is induced. In our calculation, the parameters for the D1 line of sodium atoms are used. The levels $|0\rangle$ and $|2\rangle$ (figure 1(a)) correspond to the long-lived superfine sublevels of the ground state $^2S_{1/2}$. The following values for the atomic parameters (half-widths of atomic transitions) were used: $\gamma_{10}/2\pi=10$ MHz, $\gamma_{21}=\gamma_{10}$, $\gamma_{20}=10^{-3}\gamma_{10}$. The one-photon detuning Ω_1 and the Rabi frequency G_1 are given in the γ_{10} units, $\Omega_1=-100$, the Raman detuning Ω_{20} in the units γ_{20}, and the atomic media length $L=10$ is given in the units $z_0=1/k_2\alpha_r$ (here α_r is defined by equation (A.2)), and the grating period is $\Lambda=\Lambda_x=\Lambda_y=20\lambda_1$, $w=5\Lambda$.

3.1. Near-field diffraction

Typical near-field diffraction patterns that arise under illumination of a 2D RIDG by a vortex Gaussian beam with $l=1\div 6$ are shown in figure 3 (the column number corresponds to the TC l). Here the observation plane is $z=Z_T=2(\Lambda^2/\lambda_2)$, where Z_T is the Talbot length corresponding to the classical Talbot effect [27]. The diffraction patterns are arrays of ring-like vortex beamlets (local vortices) with the period Λ that are formed at the classical Talbot distances. Colored circles indicate the positions of singular points. Red and green circles show positive and negative TC, respectively. Similar diffraction patterns are also observed in the other planes, but unlike the conventional gratings, the image in the Talbot planes is either not shifted ($z=1/2Z_T$) or shifted half the period ($z=3/4Z_T$). This is due to the properties of the Fourier coefficients of a 2D RIDG (see details in [40]). Despite the qualitative similarity of the diffraction patterns, there are significant differences for various l values. When $l=1$ each lateral (off-axis) beamlet has two singular points (figure 3(a1)). One of them is inside the ring, and the other one is located outside. The positions of singular points are determined from the condition $\Re E_2=\Im E_2=0$ [1], and their TC are defined by equation (11). The singular points inside the diffraction spots correspond to the TC of the probe field $l=1$ (figure 3(f1)). Those outside correspond to $l=-1$ as can be seen from figure 4, where a fragment of the diffraction pattern (marked by a square in figure 3(a1)) in the region of the singular point corresponding to $l=-1$ is shown. The existence of two singular points near lateral vortices physically means that there are two vortices rotating in opposite directions. In the central diffraction spot, a singular point is located in $x=y=0$ (figure 3(c1)), and the TC of this vortex is $l=1$ (figure 3(d1)).

Thus, the total TC of the lateral vortices is zero, and the total TC of the diffracted field is equal to that of the probe field (figures 5(a) and (c)). That is, the TC is conserved under diffraction on RIDG. We can say that the diffracted field is a unified (global) vortex with a singularity at $x=y=0$ with the TC equal to the charge of the probe field.

When $|l|>1$, the structure of diffraction patterns is complicated. Figures 3(a2)–(f2) shows diffraction patterns when the probe wave is a vortex with $l=2$, other parameters being the same as in the previous case. It is seen that, like in the case of $l=1$, a periodic array of ring-like beams arises with a period equal to the grating period. This array consists of local vortices with the total charge $l=2$ figures 3(a2)–(f2).

The presence of two singular points in the lateral vortices means that there arise two spatially overlapping vortices which rotate in the same direction, but their singular points are displaced relative to each other (figure 3(e2)). Therefore we see them as a single unit with a characteristic intensity distribution and the total charge $l=2$, as shown in figure 3(a2). The central vortex (in the vicinity of the point $x=y=0$) has a TC equal to the charge of the initial probe beam $l=2$ (figure 3(c2)). In addition, outside the lateral vortices, there are singular points corresponding to the charge $l=-1$. Their number is such that the total TC of the lateral vortices is zero. Thus, the diffracted field represents a global vortex with the charge $l=2$.

A completely unexpected diffraction pattern arises in the case of a probe beam with $l=3$ (figures 3(a3)–(f3)). There are five singular points inside the central vortex (figure 3(c3)). The singular point located in the center corresponds to the charge

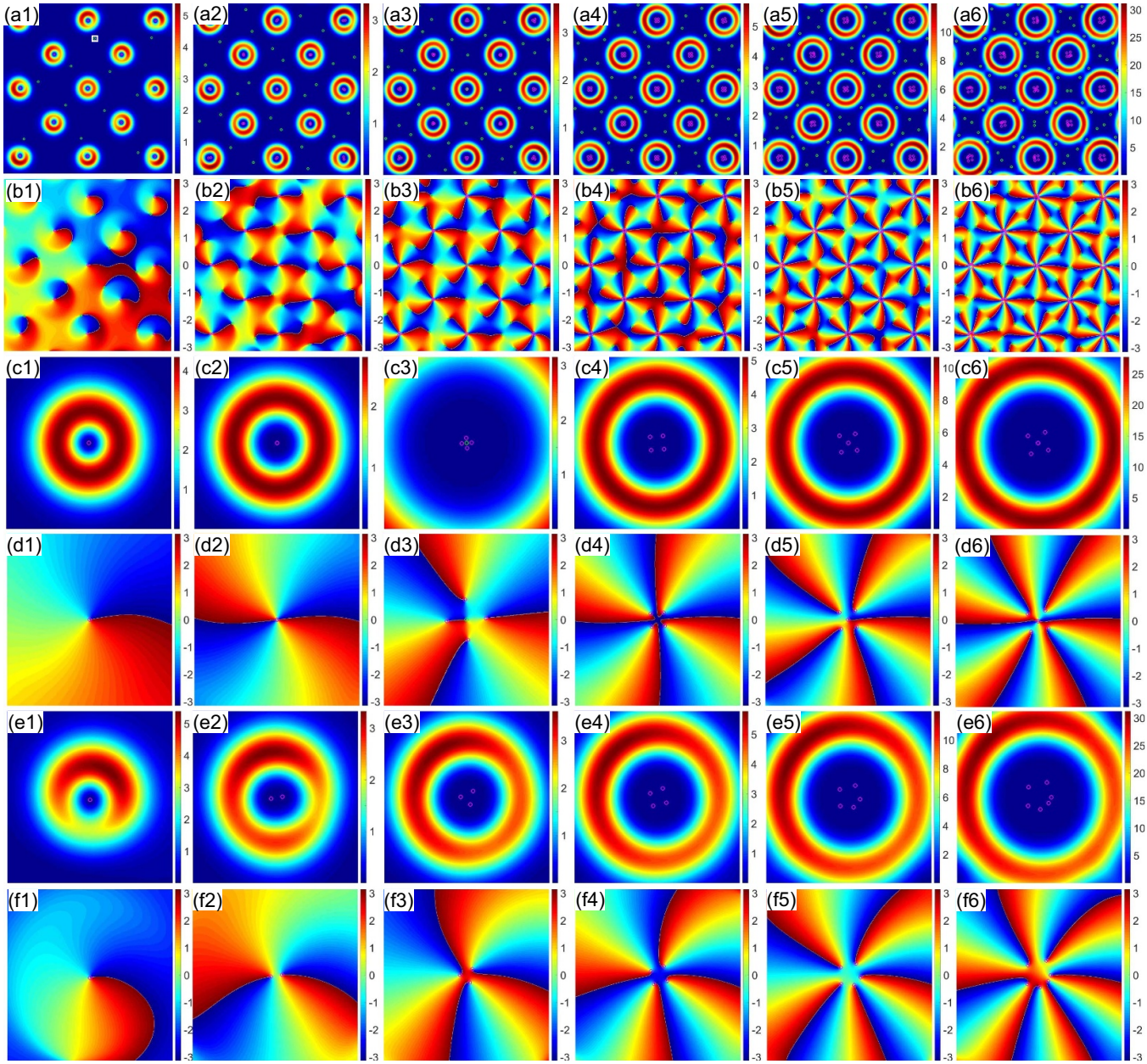

Figure 3. Intensity (a), (c), (e) and phase (b), (d), (f) profiles at the distance $z = Z_T$ for a 2D RIDG illuminated by a vortex beam with $w = 5\Lambda$, and $l = 1, 2, 3, 4, 5, 6$. (a), (b) a fragment of the central part of the diffraction pattern, (c), (d) the central ring, (e), (f) the lateral ring. The green and red circles correspond to the singular points with the negative and positive TC, respectively.

$l = -1$, and the other four points located symmetrically relative to the center have the charge $l = 1$. In contrast to the central vortex, the lateral vortices have three singular points, each with $l = 1$, as can be seen from figure 3(e3). Thus, the central diffraction spot consists of five vortices with closely spaced singular points, four of which rotate counterclockwise and one clockwise. Lateral local vortices consist of three vortices rotating counterclockwise. In addition, there are singular points, and, accordingly, vortices with the charges equal to $l = -1$ (figure 3(a3)), which compensate the charges of the local lateral vortices. As a result, the total diffraction field represents a single vortex with the TC $l = 3$ equal to the probe field's charge.

For $l = 4$, the diffraction pattern also represents an array of ring-like local vortex beams, inside which there are four singular points located as shown in figures 3(a4)–(f4). Thus, all vortex beamlets are composed of four vortices rotating counterclockwise. Besides, there are vortices with the charges $l = -1$, which rotate clockwise around these singular points. They compensate the charges of the off-axis vortices so that the total TC of the diffraction field is $l = 4$, the same as for the initial probe field. Note that a similar diffraction pattern will be observed for $|l| = 4n$, i.e. when $|l|$ is a multiple of four. For example, in the case of $l = 8$, inside the vortex beamlets, there will be eight singular points located symmetrically relative to the local vortex center and, accordingly,

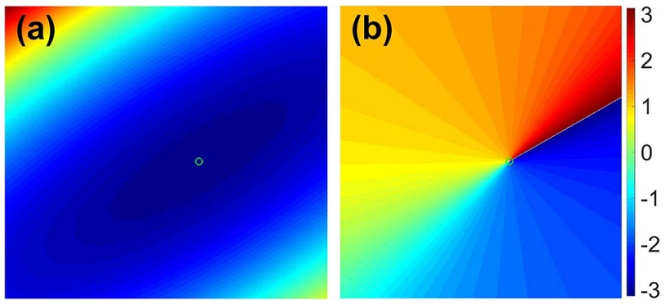

Figure 4. Intensity (a) and phase (b) profiles of the diffraction pattern near the singular point corresponding to the TC $l=-1$. In figure 3(a1) it is marked with a square.

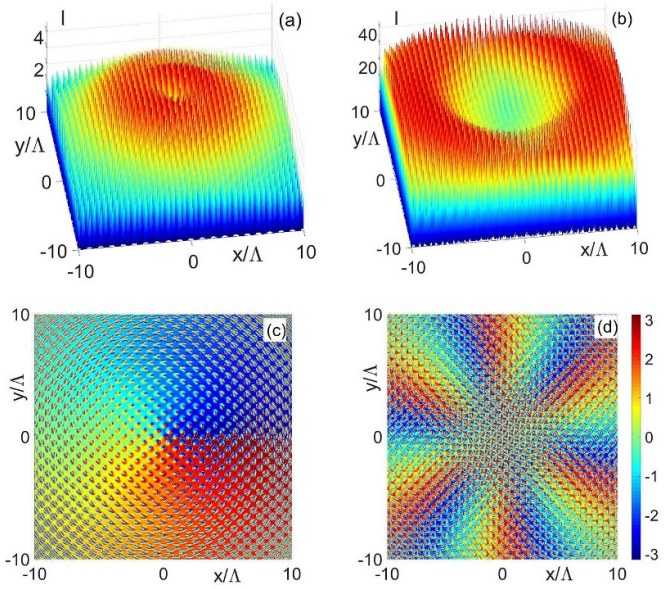

Figure 5. Illustration of an enlarged fragment of the central part of the diffraction pattern. Intensity (a), (b) and phase (c), (d) profiles of the diffraction pattern at the distance $z=Z_T$ for a 2D RIGD illuminated by a vortex beam with $l=1$ (a), (c) and $l=6$ (b), (d), $w=5\Lambda$.

all the vortices will consist of eight vortices rotating counterclockwise.

For a probe beam with $l=5$, the diffraction pattern is shown in figures 3(a5)–(f5). Inside the central local vortex (figure 3(c5)), there are five singular points, one of which is located at the point $x=y=0$. The other four singular points are located symmetrically to the center. Their respective vortices have the TC $l=1$. The lateral vortices also have five singular points inside the ring (figure 3(e5)) with the charge $l=1$. As before, in the diffracted field, there are singular points with the charge $l=-1$. They compensate for the charge of the off-axis vortices. Therefore, here the total TC of the diffracted beam is also conserved, and it is equal to the charge of the probe beam.

The probe field's diffraction patterns with the TC $l=6$ are shown in figures 3(a6)–(f6). The central vortex is similar to that for $l=5$, i.e. it contains five singular points, but the singular point in the center corresponds to the TC $l=2$, and the rest have the charge $l=1$. The lateral vortices have six singular

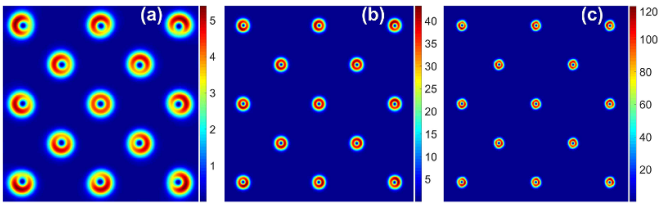

Figure 6. Diffraction patterns in the $z=Z_T$ plane for various radii w of the probe beam. (a) $w=5\Lambda$, (b) $w=10\Lambda$, (c) $w=15\Lambda$. $l=1$, $G_{10}=0.865\gamma_{10}$, $\Omega_{20}=30\gamma_{20}$.

points with the charge $l=1$. As above, there are singular points with the charge $l=-1$ which compensate the charge of the positive off-axis vortices.

Summarize the results presented in figure 3. When a 2D RIDG is irradiated by a vortex Gaussian beam, in the z = ZT plane, there arises a periodic grating of vortex beamlets with an annular intensity distribution. Note that although it has a periodic structure with the same period as the original grating, it is not the latter's self-image. The diameter of the rings in the corresponding Talbot planes depends on the probe beam's radius on the input plane of the grating, the grating period, and the TC of the illuminating beam. Expansion of the illuminating beam reduces the diameter of the rings irrespective of the charge (figure 6). The diameter grows with the number of the Talbot plane as well as with the grating period. The diameter of the rings increases with the charge l of the probe beam (figures 3(a1)–(a6)). When the sign of the charge changes, the diameter of the rings does not change.

For $|l|\geqslant 2$, each of the vortex beamlets consists of several spatially overlapping vortices so that their total TC reproduces the charge of the illuminating probe beam (figure 3). As regards the off-axis vortices ($|l|\geqslant 2$), we can say that the incident vortex beam splits into several overlapping vortices with the charge $|l|=1$, i.e. these are multi-center vortices. For the central vortices with $|l|=1,2$ such splitting does not occur, and their TC is equal to the charge of the irradiating field. Also, there are vortices having an opposite TC located outside the above beamlets; their total charge compensates for that of the off-axis vortices. Thus, we can say that under Fresnel diffraction by RIDG, the TC is conserved and that the diffracted field itself represents a single vortex (see figure 5). The results obtained are entirely consistent with the sign principle [41].

Note that when the transmission function of the grating has a glass-like shape (figure 2(b)), the diffraction patterns have a similar form.

3.2. *Far-field diffraction*

The intensity profiles of the far-field diffraction patterns under diffraction of vortex beams with different values of l are shown in figures 7(a1)–(a3). For an incident vortex probe beam with the TC l, the generated diffraction patterns are a 2D array of ring-like local vortices. These are diffraction orders of the grating, and they are formed by spatial Fourier harmonics. The spatial position of local vortices corresponds to the singular points of spatial harmonics: $b_{xn}=b_{ym}=0$ (see (14)), that is,

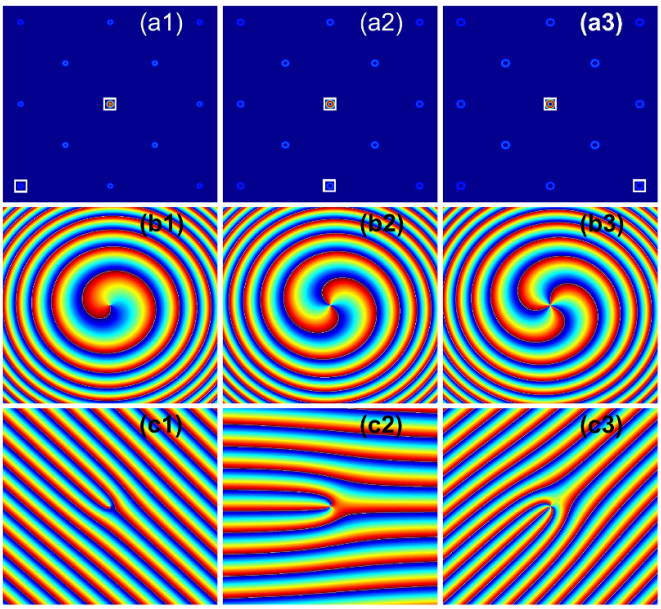

Figure 7. The first row (a_1)–(a_3): intensity profiles of the far-field diffraction patterns under illumination of a 2D RIDG by a Gaussian vortex beam with $l=1$ (a_1), $l=2$ (a_2), $l=3$ (a_3). The second row (b_1)–(b_3): phase profiles of the central diffraction spot for $l=1$ (b_1), $l=2$ (b_2), $l=3$ (b_3). The third row (c_1)–(c_3): phase profiles of the off-axis vortices marked by squares on a_1, a_2, a_3. $w=5\Lambda$, $z=5$ m. $G10=0.865\gamma_{10}$, $\Omega_{20}=30\gamma_{20}$.

their coordinates are defined as $x/z=n\lambda/\Lambda$ and $y/z=m\lambda/\Lambda$. However, since the Fourier coefficients are nonzero provided $m+n$ is even, only part of the spatial harmonics contribute to the diffraction pattern and, as a result, the 2D array of local vortices has the period $d=(2\lambda_2/\Lambda)z$. Each local vortex is a self-image of the diffracting probe beam and has a TC equal to that of the probe vortex field (figures 7(b1)–(b3) and (c1)–(c3)). Note that even though the central (figures 7(b1)–(b3)) and off-axis (figures 7(c1)–(c3)) orders have different phase profiles, their TCs are the same. Physically, this can be interpreted as follows: at these points, all other harmonics interfere destructively and do not contribute to the field. Calculations confirm this statement (figures 7(a1)–(a3)).

Surprisingly, calculation of singular points shows that in addition to the singular points given in figure 7, there is a whole group of singular points for which the TC has an opposite sign with respect to the lateral vortices. Their number is such that they compensate the charge of the lateral vortices. The charge of the central vortex remains uncompensated. Thus, the total TC of the diffracted field in the far zone is equal to the probe field's charge at the input of the grating. Figure 8 shows an example for the case of $l=2$. Additional singular points are indicated by green crosses (figure 8(a)). Moreover, in these places, two closely spaced singular points correspond to the TC with $l=-1$, as can be seen from figure 8(b), showing the square marked fragment from figure 8(a). Using formula equation (11), it is easy to verify that the total TC of the diffraction field is equal to the charge of the vortex probe field, i.e. the TC is conserved under diffraction of a Gaussian vortex beam on RIDG.

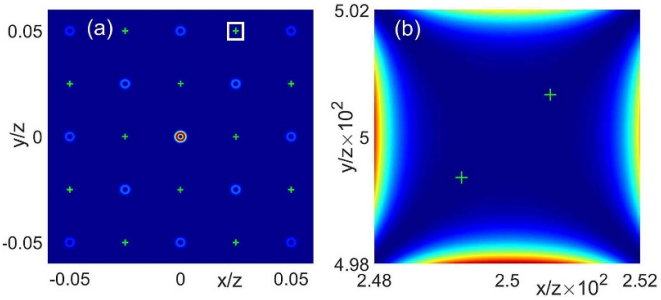

Figure 8. Far-field diffraction patterns of the vortex probe beams with $l=2$. Crosses indicate the positions of singular points, which correspond to the vortices with a negative TC.

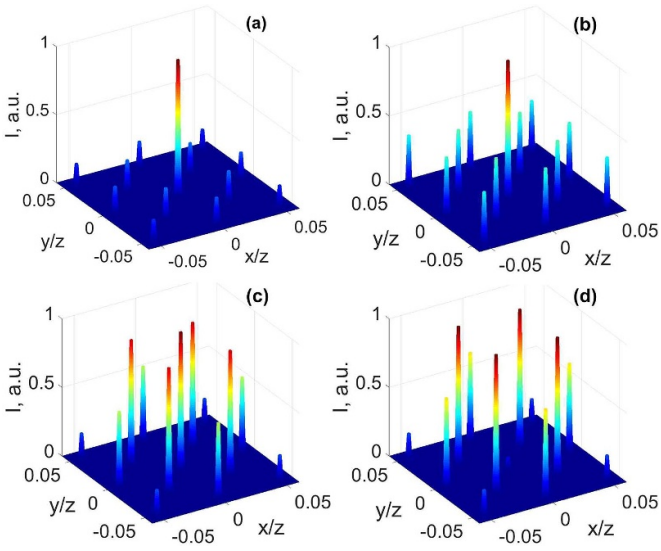

Figure 9. Far-field diffraction patterns of vortex probe beams with different values of G_1 and Ω_{20}: (a) $G_1=0.865\gamma_{10}$, $\Omega_{20}=30\gamma_{20}$, (b) $G_1=\gamma_{10}$, $\Omega_{20}=40\gamma_{20}$, (c) $G_1=1.1\gamma_{10}$, $\Omega_{20}=40\gamma_{20}$, (d) $G_1=1.2\gamma_{10}$, $\Omega_{20}=46\gamma_{20}$. $l=1$, $w=5\Lambda$, $z=5$ m.

Figure 9 displays far-field diffraction patterns of a vortex beam with $l=1$ for different Rabi frequencies G_1 and Raman detunings Ω_{20}. It shows that by choosing the parameters G_1 and Ω_{20}, diffraction orders' intensities can be effectively controlled. By changing the distance z, one can control the period of the diffraction patterns. These results show that RIDG can be used as a controllable splitting element of the incident vortex beam.

4. Conclusions

In the paper, we theoretically investigate both near- and far-field diffraction of vortex Gaussian beams on a 2D RIDG. It is shown that in the near field, diffraction patterns behind the grating are more manifold in comparison with the classical Talbot effect observed under illumination by a plane wave. The diffraction patterns (periodical structures) occur at certain distances, which correlate with the classical Talbot length. Diffraction patterns in the Talbot planes represent a 2D periodic array of ring-like vortex beamlets. Each local vortex beam has

a TC equal to that of the probe beam. Thus, upon diffraction of a vortex beam from a 2D RIDG, many vortex beams like an incident beam are produced. Although the diffraction pattern is not a self-image of the grating, it has the same nature as in the classical Talbot effect. Therefore, it can be called a quasi-Talbot image. In contrast to conventional gratings, the intensity of local vortices can be greater than the probe beam's intensity at the input of the grating due to Raman amplification in the grating. We also show that the total TC of the diffracted field is equal to the charge of the probe beam, that is, the TC is preserved under diffraction on RIDG.

It is also shown that under far-field diffraction of a vortex Gaussian beam on RIDG, a 2D periodical array of ring-like local vortices with a period depending on the z coordinate is formed. Their TCs are equal to the charge of the probe field. We found that in addition to the said singularities, there are singular points located outside the beamlets, the total charge of which is opposite to that of the lateral beamlets. As a result, the total TC of the diffracted field is equal to the probe field's charge. We also demonstrate that by choosing the pump field parameters, one can effectively control the intensity of diffraction orders.

Appendix

The induced polarization at the probe field frequency ω_2 is defined as $P(\omega_2) = \chi(\omega_2)E_2$, where $\chi(\omega_2)$ is the probe field susceptibility, and E_2 is the probe field amplitude. The susceptibility $\chi(\omega_2)$ of a three-level Λ-type atomic system for the probe field (figure 1(a)) can be derived by solving the density matrix equations, exactly for the pump field and in the first order for the probe field (weak probe field limit). In the steady-state approximation, we have [37]

$$\chi(\omega_2) = \alpha_r \frac{\gamma_{12}}{\Omega_1^2} \frac{|G_p|^2}{(\Omega_{20} + i\gamma_{20} + |G_p|^2/\Omega_1)}, \tag{A.1}$$

where

$$\alpha_r = |d_{12}|^2 N/2\hbar\gamma_{12}. \tag{A.2}$$

Here $\Omega_1 = \omega_1 - \omega_{10}$ is the one-photon detuning, $\Omega_{20} = \omega_1 - \omega_2 - \omega_{20}$ is the Raman detuning, ω_{mn}, γ_{mn} and d_{mn} are the frequency, half width, and matrix dipole moment of the transition, respectively, N is the atomic density, and $\hbar$ is the Plank constant. $G_p(x,y) = G_1[\cos(\pi x/d_x) + \cos(\pi y/d_y)]$ is the Rabi frequency of the pump field, $G_1 = d_{10}E_1/2\hbar$. The formula (A.1) is written in the approximation of $\Omega_1 = \Omega_2$. The susceptibility A.1 is spatially periodically modulated with the period $\Lambda_x = 2d_x$ and $\Lambda_y = 2d_y$. This leads to spatial modulation of the Raman gain and the refractive index. Thus, a 2D grating of the gain and the refractive index is induced in the atomic medium when a probe wave interacts with a standing pump wave.

Equation (A.1) shows that by changing the pump field intensity and frequency, one can effectively control the susceptibility $\chi(\omega_2)$. When $|G_p|^2/|\Omega_1| > \gamma_{20}$ the pump field induces an ac-Stark shift of the state $|1\rangle$, which leads to a shift of the Raman resonance by $\Omega_S = |G_p|^2/\Omega_1$ depending on the transverse coordinates.

In the approximation of a thin grating, [29], when diffraction within the bulk of the medium can be ignored, the probe field $E_2(x,y,L)$ at the output surface $z = L$ is

$$\begin{aligned} E_2(x,y,L) &= E_2(z=0)\exp(-ik_2\chi(\omega_2)L) \\ &= E_2(z=0)\exp(-k_2\chi''(\omega_2)L)\exp(ik_2\chi'(\omega_2)L). \end{aligned} \tag{A.3}$$

Here $E_2(z=0)$ is the amplitude of the probe wave at the input surface, L is the medium length, $k_2 = \omega_2/c$, $\chi'(\omega_2) = \Re\chi(\omega_2)$, $\chi''(\omega_2) = \Im\chi(\omega_2)$.

References

[1] Gbur G J 2017 *Singular Optics* (Boca Raton, FL: CRC Press)
[2] Yao A M and Padgett M J 2011 Orbital angular momentum: origins, behavior and applications *Adv. Opt. Photon.* **3** 161
[3] Kotlyar V V, Kovalev A A and Soifer V A 2014 Asymmetric Bessel modes *Opt. Lett.* **39** 2395
[4] Kovalev A A, Kotlyar V V and Porfirev A P 2016 Asymmetric Laguerre-Gaussian beams *Phys. Rev.* A **93** 063858
[5] Dennis M R, O'Holleran K and Padgett M J 2009 *Singular Optics: Optical Vortices and Polarization Singularities* (Amsterdam: Elsevier) pp 293–363
[6] Kotlyar V V and Kovalev A A 2012 *Vortex Laser Beams* (Samara: New Technology) in Russia
[7] Zhu L and Wang J 2019 A review of multiple optical vortices generation: methods and applications *Front. Optoelectron.* **12** 52
[8] Xuewen W, Zhongquan N, Yao L, Jian W, Tao L and Baohua J 2018 Recent advances on optical vortex generation *Nanophotonics* **7** 1533
[9] Rubinsztein-Dunlop H *et al* 2016 Roadmap on structured light *J. Opt.* **19** 013001
[10] Shen Y, Wang X, Xie Z, Min C, Fu X, Liu Q, Gong M and Yuan X 2019 Optical vortices 30 years on: OAM manipulation from topological charge to multiple singularities *Light: Sci. Appl.* **8** 90
[11] Willner A E *et al* 2015 Optical communications using orbital angular momentum beams *Adv. Opt. Photon.* **7** 66
[12] Yan L, Gregg P, Karimi E, Rubano A, Marrucci L, Boyd R and Ramachandran S 2015 Q-plate enabled spectrally diverse orbital-angular-momentum conversion for stimulated emission depletion microscopy *Optica* **2** 900
[13] Babiker M, Andrews D L and Lembessis V E 2018 Atoms in complex twisted light *J. Optics* **21** 013001
[14] Grier D G 2003 A revolution in optical manipulation *Nature* **424** 810
[15] Ding D-S, Zhang W, Zhou Z-Y, Shi S, Xiang G-Y, Wang X-S, Jiang Y-K, Shi B-S and Guo G-C 2015 Quantum storage of orbital angular momentum entanglement in an atomic ensemble *Phys. Rev. Lett.* **114** 050502
[16] Hebri D, Rasouli S and Dezfouli A M 2019 Theory of diffraction of vortex beams from structured apertures and generation of elegant elliptical vortex Hermite-Gaussian beams *J. Opt. Soc. Am.* A **36** 839
[17] Rasouli S and Hebri D 2019 Theory of diffraction of vortex beams from 2D orthogonal periodic structures and Talbot self-healing under vortex beam illumination *J. Opt. Soc. Am.* A **36** 800
[18] Knyazev B A and Serbo V G 2018 Beams of photons with nonzero projections of orbital angular momenta: new results *Phys.-Usp.* **61** 449

[19] Kotelnikov I A, Kameshkov O E and Knyazev B A 2020 Diffraction of Bessel beams on 2d amplitude gratings—a new branch in the talbot effect study *J. Opt.* **22** 065603
[20] Guo C-S, Lu L-L and Wang H-T 2009 Characterizing topological charge of optical vortices by using an annular aperture *Opt. Lett.* **34** 3686
[21] Tao H, Liu Y, Chen Z and Pu J 2012 Measuring the topological charge of vortex beams by using an annular ellipse aperture *Appl. Phys.* B **106** 927
[22] Zheng S and Wang J 2017 Measuring orbital angular momentum (OAM) states of vortex beams with annular gratings *Sci. Rep.* **7** 40781
[23] Dai K, Gao C, Zhong L, Na Q and Wang Q 2015 Measuring OAM states of light beams with gradually-changing-period gratings *Opt. Lett.* **40** 562
[24] Hebri D, Rasouli S and Yeganeh M 2018 Intensity-based measuring of the topological charge alteration by the diffraction of vortex beams from amplitude sinusoidal radial gratings *J. Opt. Soc. Am.* B **35** 724
[25] Panthong P, Srisuphaphon S, Pattanaporkratana A, Chiangga S and Deachapunya S 2016 A study of optical vortices with the Talbot effect *J. Optics* **18** 035602
[26] Kumar A, Vaity P, Banerji J and Singh R 2011 Making an optical vortex and its copies using a single spatial light modulator *Phys. Lett.* A **375** 3634
[27] Knyazev B, Kameshkov O, Vinokurov N, Cherkassky V, Choporova Y and Pavelyev V 2018 Quasi-Talbot effect with vortex beams and formation of vortex beamlet arrays *Opt. Express* **26** 14174
[28] Ikonnikov D A, Myslivets S A, Volochaev M N, Arkhipkin V G and Vyunishev A M 2020 Two-dimensional Talbot effect of the optical vortices and their spatial evolution *Sci. Rep.* **10** 20315
[29] Ling H Y, Li Y-Q and Xiao M 1998 Electromagnetically induced grating: homogeneously broadened medium *Phys. Rev.* A **57** 1338
[30] Wen F, Ye H, Zhang X, Wang W, Li S, Wang H, Zhang Y and Qiu C wei 2017 Optically induced atomic lattice with tunable near-field and far-field diffraction patterns *Photonics Res.* **5** 676
[31] Yuan J-P, Wu C-H, Li Y-H, Wang L-R, Zhang Y, Xiao L-T and Jia S-T 2019a Controllable electromagnetically induced grating in a cascade-type atomic system *Front. Phys.* **14** 52603
[32] Naseri T and Moradi R 2017 Realization of electromagnetically induced phase grating and Kerr nonlinearity in a graphene ensemble under Raman excitation *Superlattices Microstruct.* **101** 592
[33] Yuan J, Wu C, Li Y, Wang L, Zhang Y, Xiao L and Jia S 2019b Integer and fractional electromagnetically induced Talbot effects in a ladder-type coherent atomic system *Opt. Express* **27** 92
[34] Wen F, Wang W, Ahmed I, Wang H, Zhang Y, Zhang Y, Mahesar A R and Xiao M 2017b Two-dimensional Talbot self-imaging via electromagnetically induced lattice *Sci. Rep.* **7** 41790
[35] Arkhipkin V G and Myslivets S A 2014 Raman-induced gratings in atomic media *Opt. Lett.* **39** 3223
[36] Arkhipkin V G and Myslivets S A 2016 Coherent manipulation of the Raman-induced gratings in atomic media *Phys. Rev.* A **93** 013810
[37] Arkhipkin V G and Myslivets S A 2018 One- and two-dimensional Raman-induced diffraction gratings in atomic media *Phys. Rev.* A **98** 013838
[38] Iizuka K 2008 *Engineering Optics* 3rd ed (New York: Springer) p 532
[39] Prudnikov A P, Brychkov Y A and Marichev O I 1991 *Integrals and Series: Elementary Functions* vol 1 (London: Gordon & Breach)
[40] Arkhipkin V G and Myslivets S A 2019 Talbot effect based on a Raman-induced grating *Phys. Rev.* A **100** 063835
[41] Freund I and Shvartsman N 1994 Wave-field phase singularities: the sign principle *Phys. Rev.* A **50** 5164